Selected Area Growth Semiconductor/Superconductor Hybrid Topologically Protected Nanowire-based Networks and Planar Heterostructures (e.g. 2DEGs and 2DHGs)

Richard Kienhoefer

Supervised by: Marc Botifoll and Prof. Jordi Arbiol

Institut Català de Nanociència i Nanotecnologia (ICN2), CSIC, and BIST
11th July 2022

Semiconductor spin qubits have become an exciting avenue for scalable quantum computers, but the nanodevices that control them require further investigation to bring this excitement to fruition. By fine-tuning the strain on these devices the g-factor can be maximized and make it easier to control spin rotations for qubit gate operations, and increase spin qubit lifetimes. First, we analyzed multiple 2D electron gas (2DEG) devices, based on top down nanoengineering, using a Transmission Electron Microscope to probe into how factors such as crystal structure, strain, and composition affecting them. In Si/SiGe planar heterostructure 2DEG devices, we noted the exceedingly low density of dislocations for thinner quantum wells, as well as a larger compression imposed onto them. Secondly, we studied an alternative type of quantum devices based on planar Germanium nanowires, which follows a bottom up approach. In this latter case, strain was relieved through dislocations along the interface between the Ge wire and the Si substrate, which is thought to have been caused by the rough interface formed during fabrication as Si migrated into the Ge wire. Results for these devices have already shown better scattering properties in the heterostructures and longer coherence lengths in nanowires [RTM+22]. While the results for the nanowires already look promising, further engineering is being performed to maximize the device's potential and finally achieve 2D Hole Gas devices (2DHG).

Keywords: Electron Microscopy, Spin Qubit, Characterization

Richard Kienhoefer: Richard.Kienhoefer@icn2.cat

Acknowledgements

Special thanks to Marc Botifoll and Dr. Sara Martí for teaching me how to operate a transmission electron microscope, helping me with the device characterization, and for help and advise in writing this thesis. I would also like to thank Ramanandan Santhanu Panikar from EPFL for providing me with further information and data on their nanowires.

Contents

1 Introduction **2**

2 Background **2**
2.1 Transmission Electron Microscopy 2
2.2 Electron Signals 3
2.3 Electron Diffraction 4
2.4 Germanium Quantum Information Route 5
2.5 2D Electron Gas in Silicon Quantum Wells 6

3 Results **7**
3.1 Si/SiGe Planar Heterostructure 7
3.2 Germanium Nanowires 10

4 Conclusion & Outlook **14**

Bibliography **15**

1 Introduction

Since the Transmission Electron Microscope (TEM) was first proposed by Knoll and Ruska in 1932, the TEM has become a central tool for characterizing materials at the nanoscale, primarily between 1 and 100 nanometers [WC09]. Structures that need to be characterized with a TEM including nanowires, nanoribbons, nanoparticles, etc., composed of materials ranging from metals, alloys and ceramics to textiles and concrete. Using TEM to characterize these nanodevices opens up the possibility for in-depth analysis of atomic structure vital to the perfection and realization of spin qubits. While spin qubits are already available for industrial usage, their performance has much to be desired. The process to improve these qubits is two fold. On one hand, error correction codes are being developed to compensate for decoherence and other noise, and on the other, precise engineering in terms of atomic structure needs to be applied to maximize qubit fidelity and prolong their lifetimes. In this work, we analyzed how strain and composition affected structural characteristics of two variations of nanodevices, heterostructures and nanowires. The heterostructure's Si quantum well was isotopically purified to only contain ^{28}Si in order to reduce charge noise, therefore, it was important to understand if the inflicted strain on these isotopically pure quantum wells would cause misfit dislocations that would drastically reduce hole mobility, a key indicator for viable qubits. Furthermore, the nanowire devices were tested for lateral and horizontal defects, compositional, and overall structural characteristics.

This thesis will begin by explaining background of TEM, including emitted electron signals and electron diffraction. Section 2.4 then discusses how Germanium can be used to propagate quantum information. The background section ends with discussing the difference between a 2D electron gas and a 2D hole gas. Section 3 is split into two sections, the first is the analysis of Si/SiGe planar heterostructures and the second is an analysis of Geranium core nanowires. Finally, the thesis ends with a discussion of future directions in section 4.

2 Background

2.1 Transmission Electron Microscopy

The TEM offers many possibilities or modes to thoroughly analyze nanodevices. Distinct modes of TEM operation include High Resolution TEM (HRTEM), Scanning TEM (STEM), and Analytical Electron Microscopy (AEM). Each offering a variety of usages; STEM for instance, is good for correlating atomic species with intensities to evaluate interfaces and dislocations, while AEM uses multiple electron signals to determine chemical and structural information. Characterization of nanomaterials using these tools, or nanocharacterization, involves the imaging, measuring, and modeling of atoms.

These microscopes work by accelerating electrons through materials. Due to their wave-like property, electron waves can be passed through lenses for magnification. Electrons can achieve much shorter wavelengths than visible light whose limit is around 300nm, which allows for much greater resolution. The maximum resolution a TEM can produce is based on the wavelength of these electrons. Using the resolution distance equation:

$$\delta = \frac{0.61\lambda}{\mu sin(\beta)} \tag{1}$$

Where λ is the wavelength, μ is the refraction index, and β is the semi-angle of collection of the magnifying lens, it is shown that the smaller wavelength used the smaller the

resolution that can be achieved. Furthermore, the wavelength of electrons is dependent on the electron's energy:

$$\lambda = 1.22E^{-\frac{1}{2}} \quad (2)$$

This relationship demonstrates that the energy that the microscope accelerates the electrons at affects the resolution. The TEM adds this energy to the electrons through a voltage potential. This voltage is in terms of electron volts (eV) which modifies the equation 2 to:

$$\lambda = \frac{h}{(2m_0eV)^{\frac{1}{2}}} \quad (3)$$

Showing that the larger potential the electrons pass through the lower the wavelength the TEM can operate at. Damage to the sample can occur if the electron energy gets too high, especially to organic materials but less so in metal and semiconductor materials. Usually, semiconductors can tolerate large beam energies, therefore, they are usually visualized at 200-300 KeV to maximize resolution.

While currently electron microscopes can achieve atomic resolution with relatively low voltage requirements, electron lenses are not perfect and cause intense aberrations that dramatically reduce resolution power. Because of these aberrations and other optical defects, the maximum resolution is seldom obtained. For this reason, many compensating imaging techniques are employed in the results of this thesis.

2.2 Electron Signals

Electrons can be generated from one of two sources, thermionic or field-emission sources. A thermionic source heats up a tungsten filament or a Lanthanum hexaboride (LaB_6) crystal with a high current to provide electrons enough energy to escape the surface, the emitted electrons are then electrostatically focused with a Wehnelt cylinder as they propagate towards a hole in the anode where they are ejected. On the other hand, a field emission source produces a sharp electrical field on a tungsten tip, acting as a cathode, which allows electrons to tunnel out of when an extraction voltage is applied through the anode. When one of these sources fires an electron beam towards a specimen many signals can be produced from the interaction, show in figure 1. These signals include visible light, X-rays, transmitted and reflected electrons. Some of the important signals that are measured are characteristic X-rays for X-ray energy-dispersive spectrometry (XEDS), inelastic scattered electrons for electron energy loss spectrometry (EELS), elastic and inelastic scattering for Bragg diffraction, and Rutherford scattering for STEM signals.

XEDS can measure the x-ray spectrum emitted from the beam striking the sample. Since each element has a unique x-ray signal that generates from a photon being emitted by an electron falling from an excited state generated by the incoming electrons, those photons energies can be used for elemental composition analysis. XEDS works by counting how many times a certain energy of x-ray is measured. These counts are then used for the quantification of the stoichiometry. By configuring a small beam, less than 0.1 nm [WC09], to run across the whole sample, specific areas can be selected for instead of taking the entire sample into account.

Another more common method to analyze chemical and physical composition is EELS. EELS can analyze phonons, plasmons, as well as mapping band structure and density of states, and analyze chemical composition. Instead of measuring emitted photons and

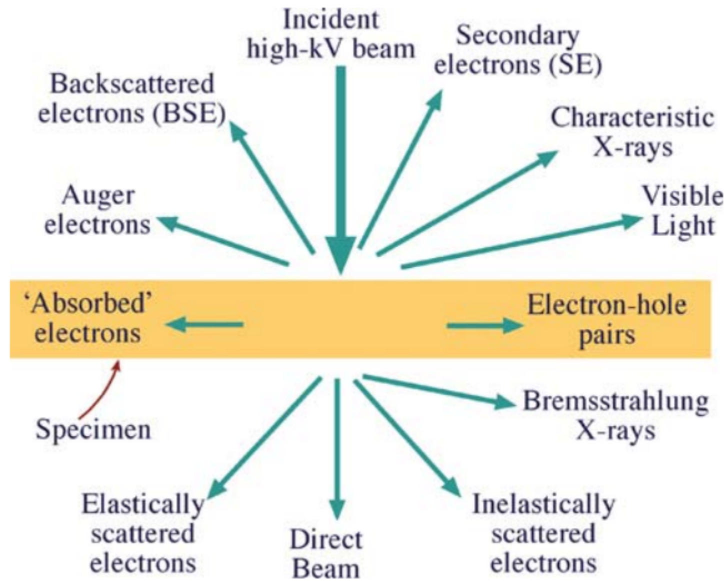

Figure 1: Electron beam interacting with a thin specimen [WC09]

counting them, this method measures what energies were lost from the transmitted electrons passing through the sample from the beam. This has the same characteristic of carrying unique energy signals as XEDS, but the energy information is carried by the electrons instead. And, like XEDS, these electrons are counted and placed on a spectrum to be analyzed. EELS is typically preferred over XEDS for its better energy resolution and amount of available information. In this thesis, EELS was used to take advantage of the higher resolution that semiconducting materials can be scanned at to map the elemental composition of the devices.

2.3 Electron Diffraction

Electron microscopes can switch to an operational mode known as electron diffraction. When the electron wave from the beam achieves a sufficiently low wavelength, the spacing between atoms are treated as a grating. This process produces a diffraction pattern which contains information about the crystal that it went through. Information like the crystals structure in reciprocal space and crystal orientation.

This process is known as Bragg diffraction described by Bragg's law. Here, when the incident angle equals the Bragg angle, a glancing angle required for interference, points of constructive interference can be observed every d^{-1}, where d is the distance between two atoms represented as atomic planes.

$$\frac{2\sin\theta_B}{\lambda} = \frac{n}{d} \tag{4}$$

These points of constructive interference led to a representation known as reciprocal space, which is the representation of a collection of parallel atomic planes, defined by a set of Miller indices (hkl). Knowing what direction, represented by [uvw], the observed crystal is oriented in allows for analysis of which other orientations are present in a crystal.

The diffraction explained above, or direct diffraction, isn't always used. Typically a Fast Fourier Transform (FFT) of the real space is used instead (compare patterns in figure 2), which is an algorithm that converts an original signal into its frequency space

representation. Both the FFT and direct diffraction patterns contain the same information of displaying the position of patterns in reciprocal space. Using the FFT instead enables precise selection and visualization of crystal orientation by utilizing the inverse FFT, which brings the FFT image back to real space.

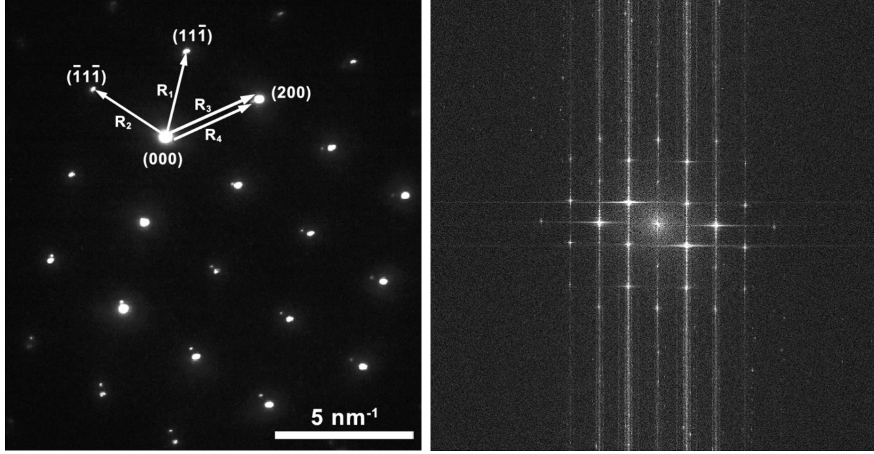

Figure 2: (a) Diffraction pattern of a Ge/Si interface [HZH+13]. (b) Fast Fourier Transform (FFT) of a Si/SiGe Heterostructure

2.4 Germanium Quantum Information Route

Germanium offers a variety of specific properties that make it fascinating for quantum computing purposes, which emerges from the potential of electron holes to channel quantum information. The low effective mass of its charge carriers allows for large energy level spacing when confined in quantum dots. Hole-spins in germanium have also shown slow relaxation times [HSH+07], necessary for their usage in qubits. The germanium platform facilitates these properties by having large and adjustable g-factors and spin-orbit interaction energies. There have been three structures identified to make use of these properties: Germanium/Silicon Core/Shell Nanowires (NW), Germanium Hut Wires (HW), and Germanium/Germanium Silicon planar heterostructures. These structural differences modify the heavy-hole (HH) and light-hole (LH) states of the germanium's band structure, specifically by engineering devices to exploit changes in them.

In bulk Ge, there are four degenerative states at the Gamma point in the electronic structure. The four degenerate states arise by combining the electrons spin degrees of freedom and the degrees of freedom from the p-type orbitals with the spin-orbit interactions. [Win03]. The eigenstates of this system are described by the Luttinger-Kohn Hamiltonian [LK55] [KTL11]

$$H_{LK} = -\frac{\hbar}{2m_0}[\left(\gamma_1 + \frac{5}{2}\gamma_s\right) k^2 - 2\gamma_s \left(\mathbf{k} \bullet \mathbf{J}\right)^2] \tag{5}$$

Where $k^2 = \mathbf{k} \bullet \mathbf{k} = k_x^2 + k_y^2 + k_z^2$, m_o is the electron rest mass, $\hbar\mathbf{J}$ is the spin 3/2 operator, and the γ terms are the material parameters. The eigenvalues of this Hamiltonian are what's known as the LH and HH states.

The first devices investigated, planar heterostructures, are an important structure to control Ge hole properties given their relative ease of growth and easy confinement requirements. The holes are confined to the strained Ge layer because of a change to the valence band close to the interface. This strained interface is caused by the mismatch in lattice

parameter between Ge and Si, which is about a 4.2% difference. This strain is controlled by creating a gradient of Ge to Si, transitioning from 90% to 60% at a rate of 10% per μm (about 3 μm), before reaching the silicon substrate [Pau10]. Due to the holes being confined to the x-y plane, the system is considered quasi-2D, creating what's known as a 2D hole gas or 2DHG. This causes the system to be sensitive to strain in the z axis, leading to large splitting of more than 100 meV between the LH and HH states [BP74]. By having a large splitting, HH states become energetically favored and therefore their effective masses become significantly lighter compared to LHs, assuming the systems spin is mainly composed of spin 3/2. The very light HH states results in reversed characteristics of LH and HH, fulfilling implementation requirements for spin qubits.

In contrast to heterostructures, nanowires require generating proximitized superconductivity through superconducting contacts, typically aluminum, to achieve its strong direct Rashba spin-orbital coupling [SDW$^+$18]. This direct coupling requires having large LH-HH mixing, which is caused by the confinement of the holes to the z-axis, or the direction of the nanowire growth, creating a 1D hole gas. The motion along this direction is described by the kinetic energy term [KTL11]:

$$\frac{\hbar^2 k_z^2}{2m_{eff}} \tag{6}$$

Where k_z is the wavevector in the z-direction and m_{eff} is the effective mass of the holes. This effective mass is also strongly dependent on compressive strain imposed by the Si shell [KTL11]. By manipulating the thickness of the Si shell, the effective mass can grow very large, reducing the kinetic energy term of the electron-electron interactions. Which has some potential usage in topologically protected devices [MML14].

One of the attractive features of electron holes is their g-factor dependence on applied electric fields. For heterostructures, a pure HH approximation suggests that there are 2 effective g-factors, $g_\perp$ and $g_\parallel$ for out of plane and in plane B field, where $|g_\perp|$ » $|g_\parallel|$. These two g-factors arise from having the magnetic field pointed in the perpendicular and parallel direction, hence the in plane and out of plane definitions. These effective g-factors depend strongly on confinement potential and magnetic field orientation, the confinement potential is based on the Zeeman splitting's g factor of $g\mu_B B$. Also, the g-factors are sensitive to mixtures of LH and HH states and therefore the assumed pure HH states in the system is insufficient to explain the entire dynamics. By having the maximum concentration of HH states, a large g-factor can be achieved, which allows for better control of the electric field and therefore the Zeeman splitting. Controlling the Zeeman splitting then, allows for control of the resonance condition of a hole-spin qubit, and for control of spin rotations.

2.5 2D Electron Gas in Silicon Quantum Wells

In contrast to the 2DHG that has been mentioned in the previous section, by substituting the Ge well with a Si well a 2D electron gas, 2DEG, can be formed instead. By using Si, a large enough conduction-band offset can be generated with sufficient strain to generate an 2DEG instead of a 2DHG. This change improves the scattering properties of the gas confined to the well reducing the charge noise. This reduced charge noise improves the lifetime of the spin qubits and would allow for longer coherence times for calculations. The goal of analyzing the Si wells in this work is to investigate how the strain and further disorders would modify this charge noise. The main drawback of using a 2DEG instead of a 2DHG is hole mobility. Recently hole mobility with Ge wells have surpassed one million $cm^2V^{-1}s^{-1}$ [DMM$^+$12] while Si wells still remain in the low 10^5, this is due to holes being significantly lighter given correct parameters.

3 Results

3.1 Si/SiGe Planar Heterostructure

Samples used are from Prof. Giordano Scappucci group at QuTech and Kavli Institute of Nanoscience in Delft. They approached creating Si/SiGe quantum dots with a top-down method, where sections of the grown heterostructure are cut to create the desired quantum dots. This approach is already wellknown and verified for its effectiveness in creating 2DEG [ECL13].

Three distinct thicknesses, 4, 6 and 8 nm, for the quantum well, QW, were characterized to understand how different well sizes affected strain parameters. Each were composed of multiple layers produced by chemical deposition. These layers in ascending order from a silicon substrate include a strain-relaxed buffer of $Si_{0.7}Ge_{0.3}$, the Si QW, 30 nm of $Si_{0.7}Ge_{0.3}$, 2 nm of a Silicon oxide cap, 10 nm of Al_2O_3, and capped off with 200 nm of an Aluminum contact, as displayed in Figure 3.1. The strain-relaxed buffer is to ensure specific strain values affecting the Si QW, since the strain affecting the Si well is based directly off the difference in lattice parameter from Si to Ge. The Si and the SiGe layers are oriented along the [110] direction of the zinc-blende structure, which shows the presence of atom pairs, known as dumbbells. Additionally, the Si QW was grown with isotopically enriched ^{28}Si as a method to further reduce charge noise caused by residual spin present in Si [DEPWF+22].

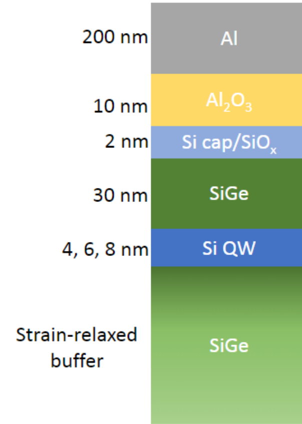

Figure 3: Outline of material layers in heterostructure device

After scanning, the wells were determined to be slightly larger than their targeted thickness. The 8 nm well was found to be roughly 9.4 nm instead.

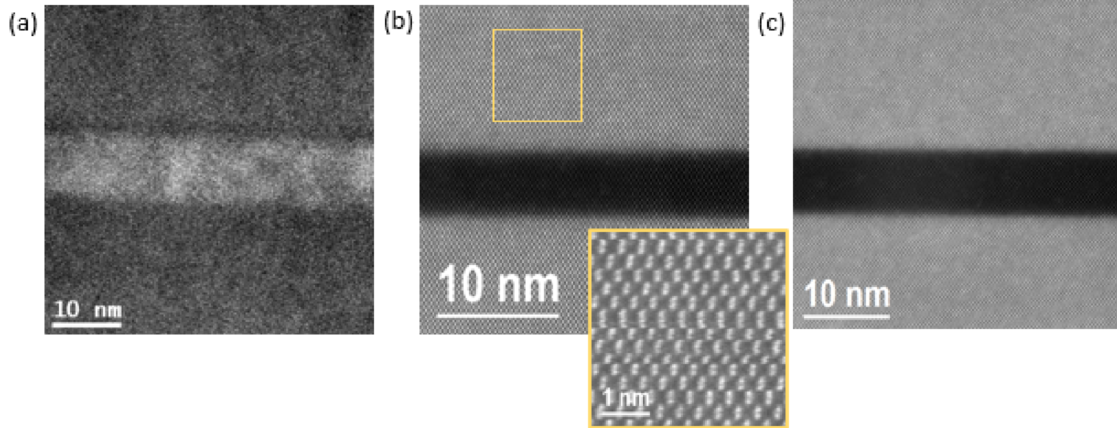

Figure 4: (a) HRTEM image of the 8 nm well. (b) STEM image of the 6 nm well. Included is a zoomed in section of the SiGE substrate, with a clear view of the SiGe dumbbells. (c) STEM image of the 4 nm well.

Composition analysis was preformed using EELS qualitative and quantitative maps, fig 5. These maps verified the percentages of Si and Ge in the well and the surrounding substrate by isolating the material signals from the extracted spectrum. In the 8 nm well, the Si content was $97\% \pm 1\%$ in the well and $69\% \pm 1\%$ ($31\% \pm 1\%$ Ge) in the SiGe layer.

What can also be seen in fig 5 is the oxygen content in the SiO_2 and Al_2O_3 layers. The SiO_2 is used to cap the Si substrate and the Al_2O_3 is used as a protective layer. Strain within the wells was analyzed using geometrical phase analysis, GPA, which calculates lattice distances from the FFT on various points on a TEM image to determine strain coefficients using variations between lattice constants. By taking the average component of the epitaxial planes and growth planes dilation of -0.17% and -1.56% respectively, and combining them with the composition percentages, the strain in the x and y directions can be calculated. This calculation is done manually, by first calculating how the composition changes substrate cell parameter using Vegard's law in the first order approximation:

$$a_{Si_xGe_{1-x}} = xd_{Si} + (1-x)d_{Ge} \tag{7}$$

where x is the percent concentration of Si, this calculates the theoretical value of the SiGe substrate and Si well. After finding the average value of the strain in the epitaxial, ϵ_{xx}, and growth planes, ϵ_{yy}, we can rearrange equation 8 to get the experimental value of the QW.

$$\epsilon_{xx} = 100\frac{d_{QW} - d_{Si}}{d_{Si}} \tag{8}$$

and finally, to calculate the distance variation of the planes, we calculate the percent difference between the theoretical and experimental interplanar distance of the QW.

$$\text{plane distance variation} = -100(1 - \frac{d_{exp,QW}}{d_{QW}}) \tag{9}$$

This calculation yields a 1% expansion in the x direction, from the left to the right of the image, and 0.39% compression in the y direction, from top to bottom. For this sample, a STEM image was unable to be taken, so strain analysis was unable to sufficiently verify dislocations or other defects.

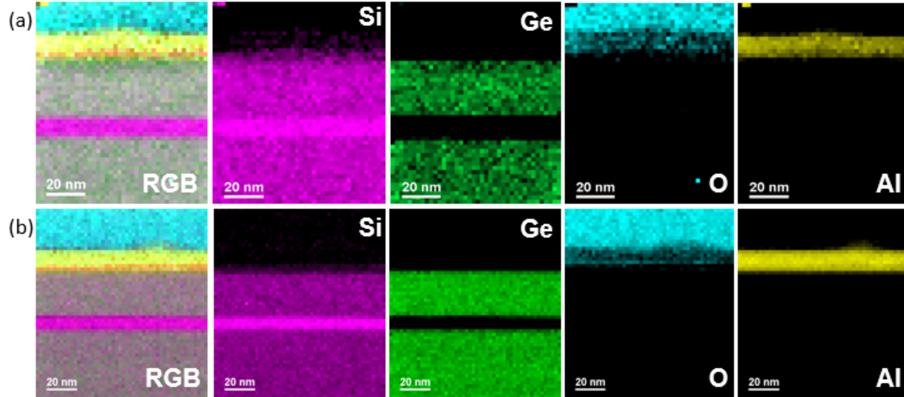

Figure 5: Difference in EELS analysis between (a) 8 nm and (b) 6 nm wells

The same pattern of a larger well width than what was aimed for is also present in the 6 nm well, with the well being 7.3 nm instead. Composition maps yielded the same results for Si percentages of $97\% \pm 1\%$ in the well and $69\% \pm 1\%$ in the SiGe layer. Strain analysis indicated no misfit dislocations along the considered section of material using the now coherent rotational strain images. With the STEM images, the magnitude of the strain in the x and y direction becomes legible. The average component of the epitaxial plane and growth planes being -0.0196% and -2.04% respectively, the calculated expansion along the x direction is 1.16% and the y direction is compressed at 0.88%.

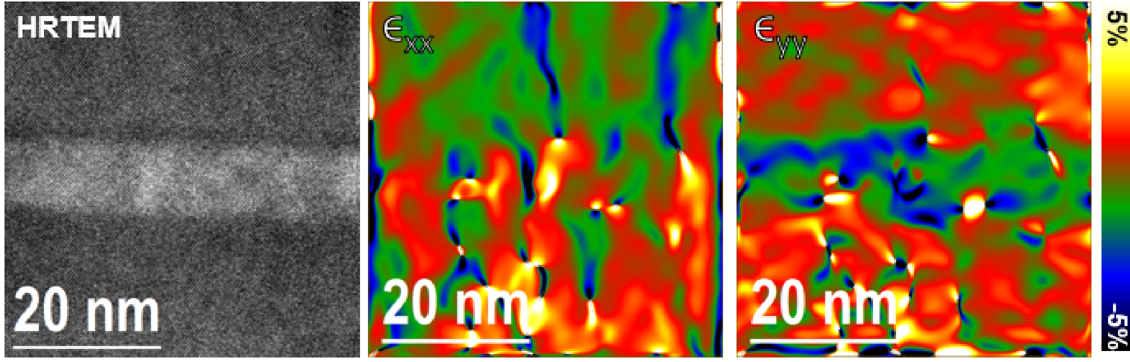

Figure 6: HRTEM image with x and y strain components for the 8 nm QW.

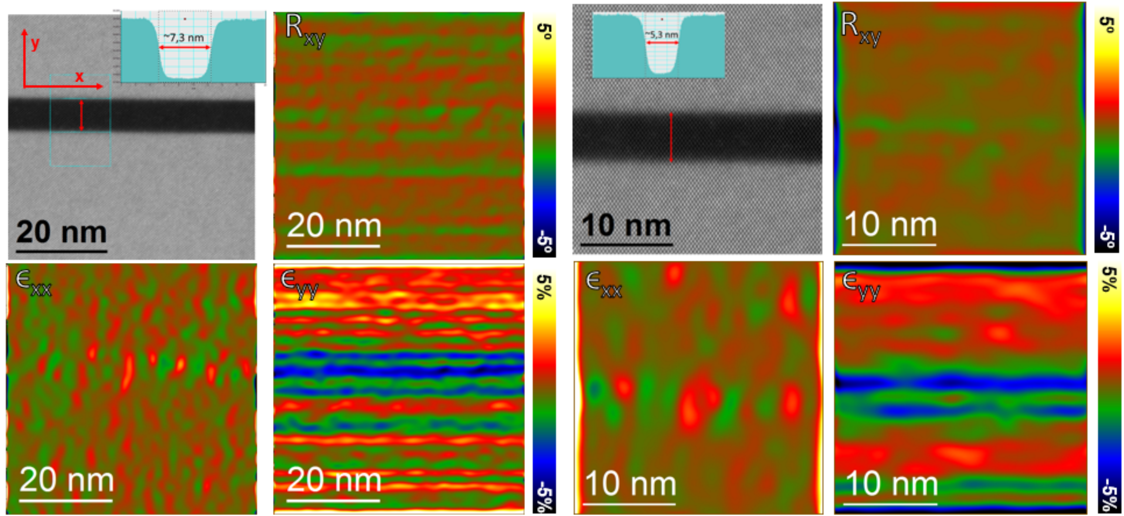

(a) Strain analysis of the 6 nm well.

(b) Strain analysis of the 4 nm well

Figure 7: For both sets of images: top left is a STEM image, top right is a rotational strain map, bottom left is the x direction strain component map, and bottom right is the y direction strain component map

Lastly, the 4 nm well contains all the previous characteristics, including that the well is a little thicker, approximately 5.3 nm. Composition maps also remain the same with the Si content in the well being $96\% \pm 1\%$ and $69\% \pm 1\%$ in the SiGe layer, see figure 6. The strain maps show similar results to the 6 nm well. The rotation maps show no dislocations in the considered section, with the average epitaxial plane component being 0.005% and the growth plane is 1.9%, the strain in the x direction is 1.14% expanded and 0.79% compressed in the y direction.

Comparing the tensile dilation in the x direction of each thickness, 1.0% 1.16% 1.14% in descending order, show that the thin wells vertical planes adapt better to the substrate. The dilation in the x direction then gives rise to the compression in the y direction as a value of the Poison distortion. This dilation is stronger in the thin wells because the strain is not being released as misfit dislocations, compared to the 8 nm well. Using the strain to calculate a new lattice parameter for the Si well and the SiGe substrate, we calculated how often a misfit dislocation may occur. One dislocation every 39.1 microns for the 4 nm well, every 9.9 microns for the 6 nm well, and every 1.1 microns for the 8 nm well. This ratio is significantly larger for the 4 nm well than the 8 nm well because of the lack of adaptation of the 8 nm well.

3.2 Germanium Nanowires

In collaboration with Prof. Anna Fontcuberta i Morral at École Polytechnique Fédérale de Lausanne, EPFL, our research group analyzed various Nanowire samples for spin qubit and topological qubit purposes. The main goal is to understand the viability of Ge/Si nanowires grown directly on a Si planar substrate, and to use these nanowires to create a scalable hole qubit network. These nanowires were grown with a bottom-up approach, by depositing Ge into an etched area of a SiO_2 mask. Four different nanostructures with various regions were characterized with variations in their growth temperature and mask size. Our characterization of these devices was focused on the strain analysis and any presence of defects, as well as other structural characteristics such as composition and faceting. Each device has four regions with two pairs of the same nanowire from the transverse and longitudinal direction, with one pair of wires grown along the [110] direction and the other grown along the [100] direction.

One such sample with a SiO_2 mask size of 25 nm, grown along the [100] direction, was shown to have two different intensities, see figure 8. By utilizing the FFT to isolate the specific periodic structure of Ge from the image of the wire, demonstrates that the varying intensities in the nanowire are caused by focused ion beam, FIB, amorphization. This is also revealed again in the compositional analysis where the Ge is present in both sections. Another damage to the sample is the sinking of the Ge into the Si interface. A small hole is dug up into the Si substrate while etching into the SiO_2 mask.

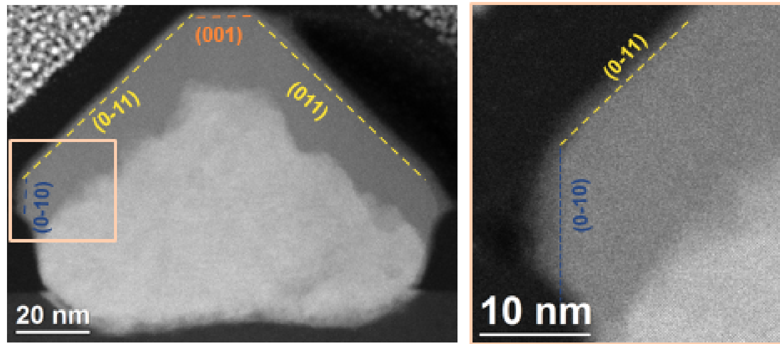

Figure 8: Nanowire A. In the amorphized section different facets can be made out. These facets are due to the growth orientation, mask size, and growth area.

The other interesting section on these wires is the bottom interface with the Si (001) substrate. Here the interface is rough due to the Si migrating into the Ge nanowire. This is again further exemplified in the compositional analysis, fig 9b.

Strain relaxation for the wires come from a few additional mechanisms than just lattice mismatch. Firstly, misfit dislocations between the wire and the substrate are clearly visible with the strain rotation maps as sharp variations along the interface. In these wires, the Ge grows beyond the top of the mask. This can create an additional vector of strain relief when the growing wire begins to rotate outwards [KSA+18]. These samples were absent of this extra rotational relief, instead figure 9c shows a slight, smooth plane rotation as an elastic strain relaxation mechanism.

Viewing the wire in the horizontal orientation further demonstrates the roughness that is plaguing growth, Fig 10. Dislocations were also more obvious by viewing the strain images horizontally as well. This horizontal view also allowed us to analyze whether other defects were present along the wire that would not have been seen from the vertical view. We observed a plane twinning, where two planes have mirrored symmetries to each other,

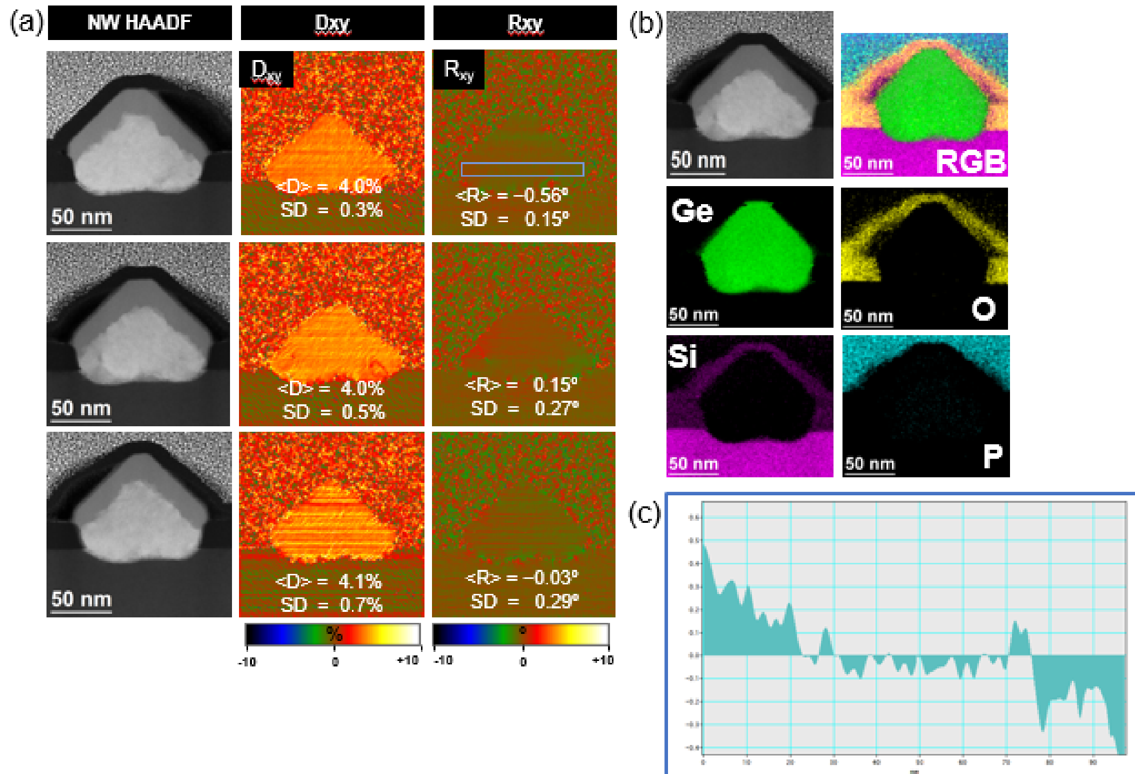

Figure 9: (a) Multiple samples of Nanowire A with accompanying strain maps (b) Composition of Nanowire A (c) Graph showing how rotational strain evolves across Nanowire A indicated with by blue rectangle in section (a).

going diagonally across the wire in figure 10. Typically, this cannot be directly viewed when oriented in the (010) direction, as this orientation is in, but we can extrapolate this occurrence through an intensity difference in the strain analysis.

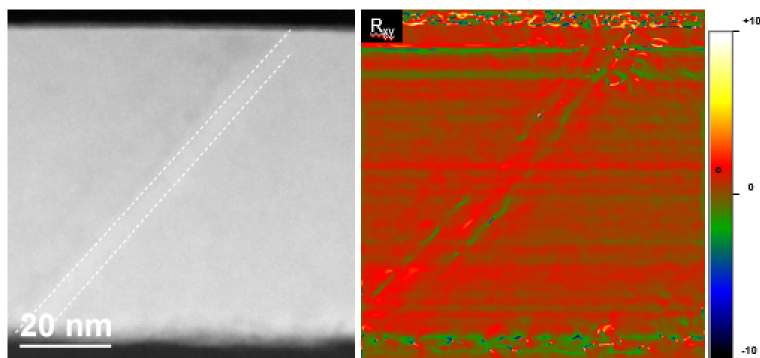

Figure 10: Horizontal section of Nanowire A. White dashed line indicates area of twin plane. Right image demonstrates outcome of the twin plane on rotational strain.

In the same set of devices, the nanowire grown in the [110] direction had very different physical characteristics than the nanowire grown in the [100] direction. These wires, shown in figure 11, were rounder with less distinct facets. While the same problems of Si migration were still present, these devices had much clearer dislocations in the strain maps, figure 12.

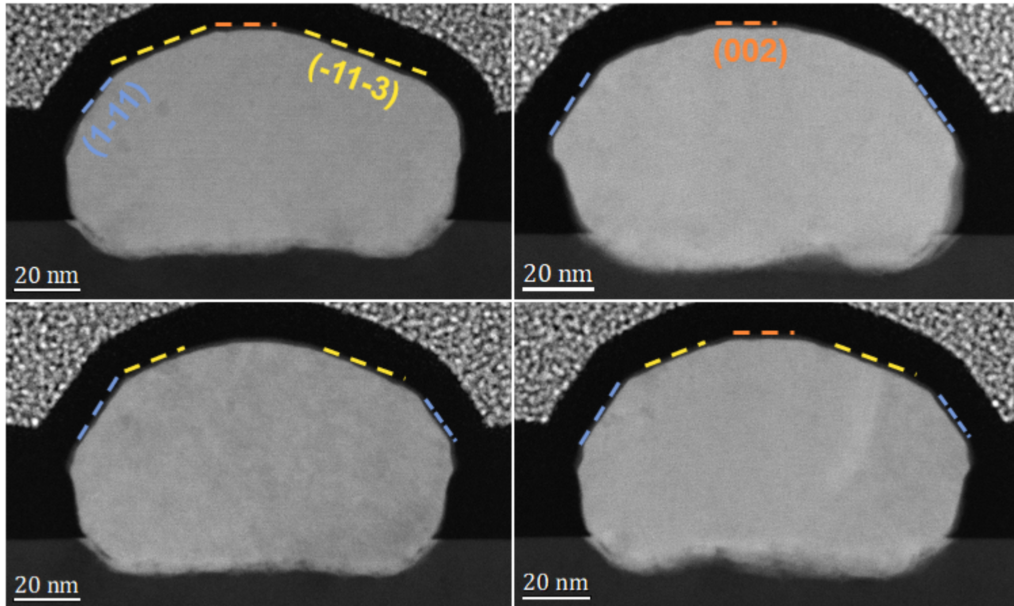

Figure 11: Four distinct wires grown in the [110] direction. Orange dashed lines indicate (002) facets, blue dashed lines indicate (1-11) facets, and yellow dashed lines indicate (-113) facets. While areas with no facet indications could not be resolved enough to label.

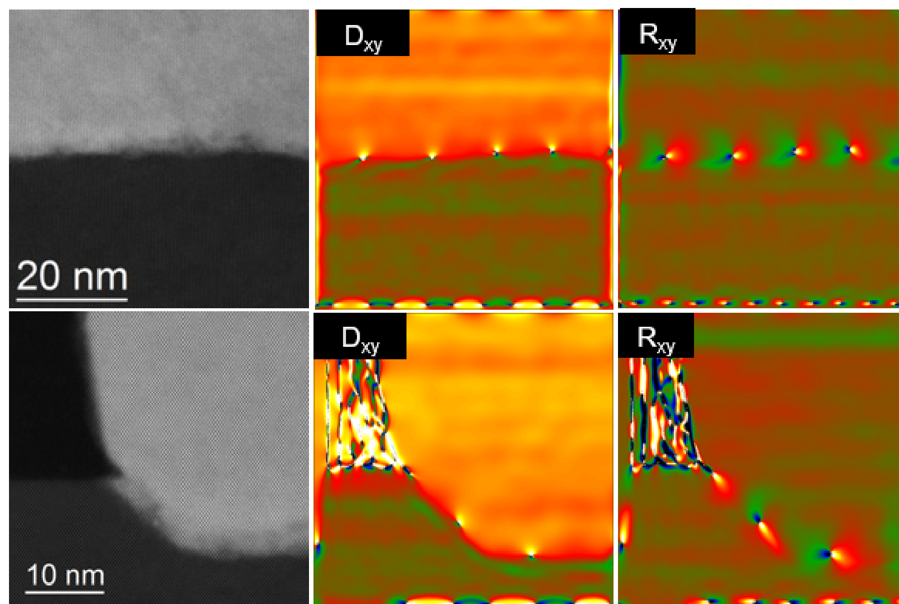

Figure 12: Strain analysis from two different sections from the [110] Nanowire. Rotation maps demonstrate misfit dislocations on the bright areas along the interface.

Beyond the two different wires shown in this paper, six more variations of similar nanowires with varying parameters, mainly in temperature growth and SiO_2 mask depth, were also analyzed but not included in this work. A common trend in these wires was that the higher growth temperatures gave enhanced crystal quality than the lower ones. The samples in this thesis were also measured at room temp for normalized conductance as a function of the width of the nanowires, fig 13. These measurements are on par with previous measurements with the primary difference being a smaller hole concentration [RTM+22].

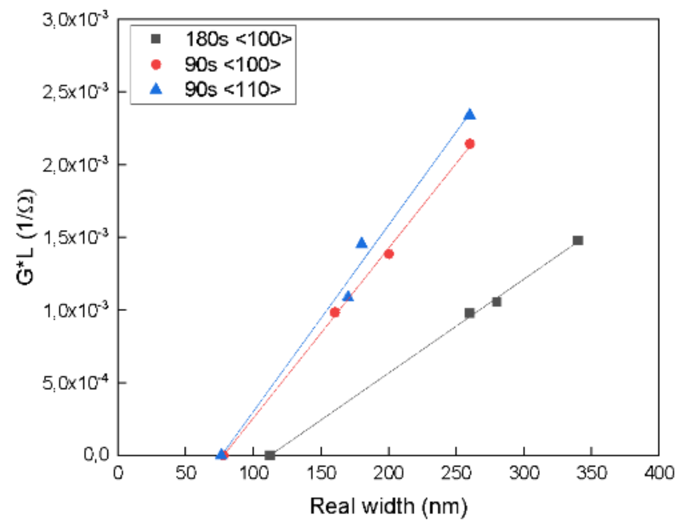

Figure 13: Normalized conductance as a function of nanowire width. 180 and 90 labels correspond to growth times of the wires.

4 Conclusion & Outlook

From this analysis of nanowires and quantum wells, both type of devices maintains to stay contenders for scalable qubit applications. Composition and strain analysis are in appropriate ranges for these devices to work. With optimized strain applied to the QW's and the isotopically purified ^{28}Si, not only enables the desired 2DEG but also minimizes misfit dislocations that siphon electron and hole mobility and maximizes scattering properties.

Testing of the QWs ability to maintain quantum information [DEPWF+22] revealed an improvement to mobility of the 2D electron gas. This improvement was directly linked to the reduced dislocations from utilizing thinner wells, as well as the purity of ^{28}Si. These improvements then led to significantly reduced charge noise and improved scattering properties.

In comparison to the highly researched planar 2DEG heterostructures, integrated nano wires have not been as deeply researched. It was theorized that quantum dots could be grown on top of the nanowire grids to facilitate scalable qubit networks, but this could not be realized due to the lack of selectivity for growing the quantum dots above the networks. These nanowires present a new research direction that this thesis helps facilitate progress in by indicating where the devices fall short of meeting theoretical standards. Some challenges with growing these nanowires were to create a smoother interface with the Si substrate, as indicated in the nanowire compositional analysis. In a discussion I had with Ramanandan Santhanu Panikar, a doctoral assistant at EPFL, he indicated that one way they wanted to addressed this roughness is with the addition of a thin layer of aluminum into the etched well before depositing the Ge. On top of addressing the roughness, the team at EPFL are also decreasing the width of the wires from 90 nm to 35 nm. A smaller width would allow them to probe further into nanowires capabilities as spin qubits. All these changes to the nanowire growth I will be continuing to characterize for my PhD.

Nanowire nodes are points where multiple nanowires intersect. At these points strain, compositional, and crystal structure characterization will have to be performed to ensure proper transmission of quantum information. This serves as another point of interest in future work.

Bibliography

[BP74] Gennadii Levikovich. Bir and Grigorii Ezekielevich Pikus. *Symmetry and strain-induced effects in semiconductors [by] G. L. Bir and G. E. Pikus. With foreword by J. C. Hensel. Translated from Russian by P. Shelnitz. Translation edited by D. Louvish.* Wiley New York, 1974.

[DEPWF+22] Davide Degli Esposti, Brian Paquelet Wuetz, Viviana Fezzi, Mario Lodari, Amir Sammak, and Giordano Scappucci. Wafer-scale low-disorder 2DEG in ^{28}Si/SiGe without an epitaxial si cap. *Appl. Phys. Lett.*, 120(18):184003, May 2022.

[DMM+12] A. Dobbie, M. Myronov, R. J. H. Morris, A. H. A. Hassan, M. J. Prest, V. A. Shah, E. H. C. Parker, T. E. Whall, and D. R. Leadley. Ultra-high hole mobility exceeding one million in a strained germanium quantum well. *Applied Physics Letters*, 101(17):172108, 2012.

[ECL13] M A Eriksson, S N Coppersmith, and M G Lagally. Semiconductor quantum dot qubits. *MRS Bull.*, 38(10):794–801, October 2013.

[HSH+07] D Heiss, S Schaeck, H Huebl, M Bichler, G Abstreiter, J J Finley, D V Bulaev, and Daniel Loss. Observation of extremely slow hole spin relaxation in self-assembled quantum dots. *Phys. Rev. B Condens. Matter Mater. Phys.*, 76(24), December 2007.

[HZH+13] Yourui Huangfu, Wenbo Zhan, Xia Hong, Xu Fang, Guqiao Ding, and Hui Ye. Heteroepitaxy of ge on si(001) with pits and windows transferred from free-standing porous alumina mask. *Nanotechnology*, 24(18):185302, May 2013.

[KSA+18] Filip Krizek, Joachim E. Sestoft, Pavel Aseev, Sara Marti-Sanchez, Saulius Vaitiekėnas, Lucas Casparis, Sabbir A. Khan, Yu Liu, Toma š Stankevič, Alexander M. Whiticar, Alexandra Fursina, Frenk Boekhout, Rene Koops, Emanuele Uccelli, Leo P. Kouwenhoven, Charles M. Marcus, Jordi Arbiol, and Peter Krogstrup. Field effect enhancement in buffered quantum nanowire networks. *Phys. Rev. Materials*, 2:093401, Sep 2018.

[KTL11] Christoph Kloeffel, Mircea Trif, and Daniel Loss. Strong spin-orbit interaction and helical hole states in Ge/Si nanowires. *Phys. Rev. B Condens. Matter Mater. Phys.*, 84(19), November 2011.

[LK55] J M Luttinger and W Kohn. Motion of electrons and holes in perturbed periodic fields. *Phys. Rev.*, 97(4):869–883, February 1955.

[MML14] Franziska Maier, Tobias Meng, and Daniel Loss. Strongly interacting holes in Ge/Si nanowires. *Phys. Rev. B Condens. Matter Mater. Phys.*, 90(15), October 2014.

[Pau10] D J Paul. The progress towards terahertz quantum cascade lasers on silicon substrates. *Laser Photon. Rev.*, 4(5):610–632, September 2010.

[RTM+22] Santhanu Panikar Ramanandan, Petar Tomić, Nicholas Paul Morgan, Andrea Giunto, Alok Rudra, Klaus Ensslin, Thomas Ihn, and Anna Fontcuberta i Morral. Coherent hole transport in selective area grown ge nanowire networks. *Nano Letters*, 22(10):4269–4275, 2022. PMID: 35507698.

[SDW+18] Jian Sun, Russell S Deacon, Rui Wang, Jun Yao, Charles M Lieber, and Koji Ishibashi. Helical hole state in multiple conduction modes in Ge/Si core/shell nanowire. *Nano Lett.*, 18(10):6144–6149, October 2018.

[WC09] David B Williams and C Barry Carter. *Transmission electron microscopy.* Springer, New York, NY, 2 edition, January 2009.

[Win03] Roland Winkler. *Spin-orbit coupling effects in two-dimensional electron and hole systems*. Springer tracts in modern physics. Springer, New York, NY, December 2003.